SAIL TRIMMING FSI SIMULATION - COMPARISON OF VISCOUS AND INVISCID FLOW MODELS TO OPTIMISE UPWIND SAILS TRIM

M. Sacher[1], matthieu.sacher@ecole-navale.fr
F. Hauville[1], **P. Bot**[1], **M. Durand**[2]

Abstract. A numerical comparison between two FSI models, based on inviscid and viscous flow solvers, is presented in this paper. The differences between aerodynamic coefficients, sail flying shape and pressures computed by both FSI tools are investigated for medium wind conditions. These differences are evaluated for different values of the main sheet length. The study has shown very close results when the main sheet is not over trimmed for medium true wind speed, but discrepancies increase when flow separation becomes significant. Then, an optimisation procedure based on inviscid FSI is performed to optimise the main sheet and car trims, in order to maximise an objective function based on the driving and side forces, in a case of low true wind speed. Limitations of the inviscid flow hypothesis are highlighted and the difficulties to use inviscid FSI models in an optimisation procedure, for a case of low true wind speed, are shown.

NOMENCLATURE

Cx	-	Driving force coefficient
Cy	-	Side force coefficient
Cmx	-	Heeling moment coefficient
$\triangle C_P$	-	Pressure difference coefficient
ZCE	m	Center of aerodynamic forces height
S_{ref}	m^2	Reference sail area
BS	m/s	Boat speed
TWS	m/s	True wind speed
AWS	m/s	Apparent wind speed
TWA	deg	True wind angle
AWA	deg	Apparent wind angle

1. INTRODUCTION

The research field of sailing yachts has been growing in the last decades. Particularly for the Fluid-Structure Interaction (FSI) applied on sails [1–3]. The *Naval Academy Research Institute* has contributed to this research and has performed numerical and experimental validations [4, 5]. These developments lead to improve the modelling, and FSI tools can now be used to increase the performance of sailing yachts.

The performance is usually studied by using numerical methods. Most of the racing teams are using Velocity Prediction Programs (VPP) [6] in order to evaluate the Velocity Made Good (VMG) of the boat. A VPP is a program which solves the yacht equilibrium by balancing forces from hull, appendages and sails. Forces can be based on empirical formulations, experimental data or numerical calculations [7], in order to create aerodynamic or hydrodynamic matrices of data, and sometimes it is used in real time, in a wind tunnel [8]. Developments have also been performed on Dynamic VPP [9–11].

The study of sailing yachts performance can focus on hydrodynamics [12, 13] and aerodynamics. Improving sails is a very complex problem. It is subject to highly coupled FSI effects and instabilities. Moreover, modelling the fluctuating real sailing conditions is still a research field and the effects of uncertainty in the input wind and sea state are difficult to estimate. Therefore, currently, the optimal shape of sails is studied without taking into account the FSI part [14], or the study of the trimming is done on 2D problems [15]. Some recent studies have been done on the performance by using FSI calculations with an inviscid flow solver on a VPP, taking into account the trimming of sails [16].

Differences in FSI calculations results computed by two FSI models: ARAVANTI and ARA-ISIS which are using inviscid and viscous flow solvers respectively are investigated. The differences on the aerodynamic coefficients and the shape of sails are highlighted. Calculations have been done on a Figaro Class yacht for different trims of the main sail. An optimisation procedure has been performed for a case of low true wind speed. The inviscid flow solver was used to optimise the sail trim and this "inviscid optimum" was then evaluated by the viscous flow solver.

The paper is organised as follows. Section 2 presents the numerical methods, numerical models, FSI procedures, simulations set-up and post-processing. In Section 3, results from both models are compared in medium wind conditions. Section 4 presents an optimisation procedure of the mainsail trim in light wind conditions. Finally, the last section gives some conclusions and perspectives for further work.

[1]Naval Academy Research Institute-IRENav, France
[2]K-EPSILON Company, France

2. NUMERICAL METHODS

2.1 Numerical Models

The structural solver ARA has been developed by *K-EPSILON* during the VOILEnav project [4]. The code is able to simulate a sail boat rig by using various structural elements such as Timoshenko beams, cables, or constant strain triangles (CST) membrane elements, to model several types of sails: 3DL, 3DI, D4, etc.

The code is coupled to the inviscid flow solver AVANTI for steady or unsteady simulations [1]. AVANTI is based on the Vortex Lattice Method (VLM). Sails are composed of rectangular panels associated with doublets where the slip condition is imposed. A vortex particle model is used for the wake and the Kutta condition, which is imposed at the trailing edge, is used to calculate the lift of sails. The model is supposed to be valid for an attached flow, i.e. low-camber profiles at low angle of attack.

ARA is also coupled to the URANS ISIS-CFD solver (FINE^{TM}/Marine software) [1, 2]. ISIS-CFD is developed by the *DSPM* team from the *LHEEA* laboratory. The code solves the Reynolds-Average Navier-Stokes Equations (RANS). It is based on the finite volume method and works with structured and unstructured meshes. Several turbulence models are implemented in the solver. The ALE (Arbitrary Lagrangian Eulerian) formulation of the equations is used to take into account the mesh deformations.

The global FSI resolution algorithm is based on a quasi-monolithic approach developed by Durand [1]. It is an implicit coupling adapted to a partitioned solver. The solution of the structure problem is included in the fluid solving loop, and is achieved for each fluid iteration. The convergence properties and stability of the monolithic approach is conserved.

In the ARAVANTI calculations, the fluid mesh part is only a surface composed of rectangular panels which correspond to the sail. In the ARA-ISIS computations, the fluid domain (box around the sails) is meshed. When the structure is deforming, the fluid mesh has to be deformed as well. This is done by using a mesh deformation propagation method. The deformation is propagated to all nodes step by step from the interface to the edges of the fluid domain.

Both FSI codes, ARAVANTI and ARA-ISIS are able to simulate a sail boat rig in order to predict global forces, local deformations and the shape of sails according to the loading conditions. Coupled models have been validated at the *Naval Academy Research Institute-IRENav* by using numerical and experimental comparisons (see [1, 4, 5]). For more information on the structural or fluid solver, the reader is referred to references [1, 17, 18].

2.2 Numerical Sail Boat

Sails have been designed by *All Purpose*, using the SailPack software, developed by *BSG Développements*. Fiber orientations and mechanical characteristics are taken into account: see Figure 1. Dimensions and mechanical characteristics of the mast, boom, etc. are provided by the company *Sparcraft*. The basic tuning of the mast is done according to the values used by the *Figaro Class*.

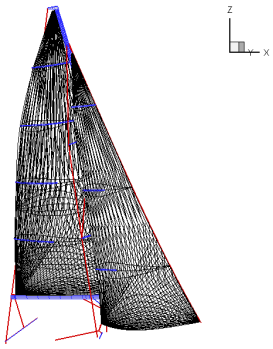

Figure 1. Numerical Figaro II

The reference coordinate system shown on Figure 1 is used for computations. X, Y and Z axis are attached to the earth North, West and local Vertical respectively. The yacht is heading north. The center of the reference coordinate system is defined as follows: $X = 0$ at the yacht center of gravity longitudinal position; $Y = 0$ on yacht centreline; $Z = 0$ at the sea level for an upright yacht.

2.3 FSI Procedures

FSI computations on sails are difficult and require a precise procedure in order to get converged and accurate calculations.

The FSI procedure to reach a converged result with ARAVANTI is explained below.

1. A structural computation on the rig without the sails is done, corresponding to the static tuning of the rig.
2. Sails are added to the rig and the structural and inviscid fluid meshes are generated by ARAVANTI.
3. A first FSI computation is done with a uniform pressure on the sails in order to position the sails on the rig with a first deformed shape.
4. The calculation with the inviscid fluid is finally computed in a steady case. This leads to a flying shape.

Once the first result is reached, it becomes the reference point and a new computation with a new trim can be run with a restart from the reference point (the new computation starts from step 4).

The FSI procedure used with the ARA-ISIS tool starts from step 4.

4.1 A fluid domain is generated around the deformed sail.

4.2 The mesh is created with HEXPRESS^{TM}, a semi-automated mesh generator (included in the FINE/Marine^{TM} software package) based on the octree method. Figure 2 shows the red and blue lines which are the inlets (far field) and outlets (frozen pressure) respectively. A symmetry condition is applied at the sea level ($z = 0$ m) and a zero pressure gradient is imposed on the top mesh face.

4.3 A fluid convergence begins before the FSI iterations in order to initialise the flow field.

4.4 FSI iterations are computed and the fluid mesh is deformed in each sub-iteration of coupling.

As before, when the convergence is reached, the result becomes the reference point. If a new calculation is needed, the new one restarts from step 4.4 and the mesh is naturally deformed with the FSI tools.

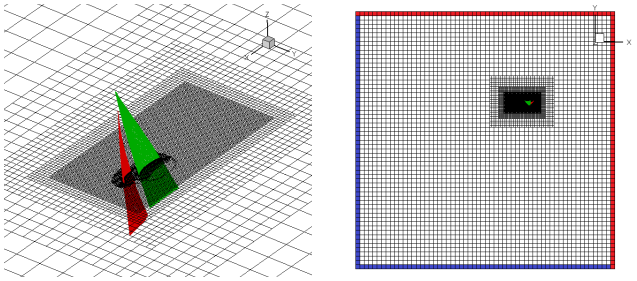

(a) (b)

Figure 2. Fluid mesh (viscous FSI computations)

2.4 Computation Parameters

The domain size is equal to 200 m, 200 m and 60 m for respectively X, Y and Z directions of the mesh.

The leading edge separation on the main sail due to the mast is not computed by ARAVANTI. Therefore, the mast has not been meshed in the ARA-ISIS simulations in order to get very close comparisons. The mesh uncertainty [19] has not been verified in this study. Two meshes of fluid for the viscous model (about 1.5 and 2 million cells) have been tested with refined cells close to the sails, in order to get a $y+ = 80$, to permit using a wall function boundary conditions, and close to the sea level in order to correctly capture the wind velocity profile. The used mesh is the one with about 2 million cells. For the inviscid fluid, one mesh has been used made of about 380 surface elements. In both cases, inviscid or viscous FSI simulations, the structural mesh is identical and the number of membrane elements is about 4500.

Viscous FSI calculations have been performed using the $SST\ k-\omega$ [20] turbulence model on 24 CPU. The computing times was about 6 hours and 20 minutes for the ARA-ISIS and ARAVANTI simulations respectively.

Simulations are steady (quasi-static approach) and a logarithmic vertical wind profile with a reference velocity at 10 m height and $z_0 = 0.2$ mm is used [21] (see Equations (1 – 2)).

$$TWS(z) = TWS_{10\text{m}} \frac{\ln\left(\frac{z}{z_0}\right)}{\ln\left(\frac{10}{z_0}\right)} \tag{1}$$

$$AWS(z) = \sqrt{(TWS(z)\cos(TWA_{10\text{m}}) + BS_{10\text{m}})^2 + \overline{(TWS(z)\sin(TWA_{10\text{m}}))^2}} \tag{2}$$

The aerodynamic forces matrix is computed at the center of gravity of the yacht. Results presented in this paper are the fluid components of the forces matrix.

2.5 Post-Processing

The aerodynamic coefficients Ci and Cmi (with i the considered axis) are computed by:

$$Ci = \frac{Fi}{\frac{1}{2}\rho S_{ref}(AWS_{10\text{m}})^2} \tag{3}$$

$$Cmi = \frac{Mi}{\frac{1}{2}\rho S_{ref}^{(3/2)}(AWS_{10\text{m}})^2} \tag{4}$$

With,

S_{ref}: the reference sail area, 34 m^2

ρ: the air density, 1.225 kg/m^3

$AWS_{10\text{m}}$: the apparent wind speed at 10 m computed by taking into account the heel angle effect [22]

The difference of pressure $\triangle P$ and the associate coefficient $\triangle C_P$ are computed by:

$$\triangle P = P_{leeward} - P_{windward} \tag{5}$$

$$\triangle C_P = \frac{\triangle P}{\frac{1}{2}\rho(AWS_{10\text{m}})^2} \tag{6}$$

3. INVISCID AND VISCOUS FSI COMPARISON

In this Section, the influence of the main sheet trim on the aerodynamic coefficients is presented. Nine values of the main sheet length have been tested by using both ARAVANTI and ARA-ISIS computations. All other trim settings are fixed and identical in the eighteen FSI calculations.

Then, two main sheet trimmings are chosen and differences on the sail shape and the pressure difference coefficient are presented.

Sailing conditions have been given by the *Figaro Class* and they are identical for all computations. Boat speed is fixed to 6.2 kts, the true wind speed at 10 m height is 15 kts and the true wind angle is equal to 40 deg on port tack. The trim, heel and heading angles are 0, 20 and 0 deg respectively. Therefore, $AWS_{10\text{m}} = 19.88$ kts.

3.1 Aerodynamic coefficients

Figures 3 – 5 show the total aerodynamic coefficients Cx, Cy and Cmx, computed with the inviscid and viscous FSI solvers versus the main sheet length. The main car position is 24.2 cm to windward from the yacht centerline for all cases.

The differences are maximized when the main sheet is over trimmed in (short main sheet length). In this configuration, all the aerodynamic coefficients are higher according to the inviscid model ARAVANTI. When the sheet is eased out, the differences, for Cx and Cmx, decrease until a main sheet length of 1.55 m and finally, the differences are almost constant on the last 3 points. For these points, the differences are about 7% and 0% for Cx and Cmx respectively. For Cy, the difference is decreasing as well, and vanishes at a sheet length of 1.45 m. Then, the difference increases and Cy is higher according to the viscous model ARA-ISIS (the constant difference is about 4%).

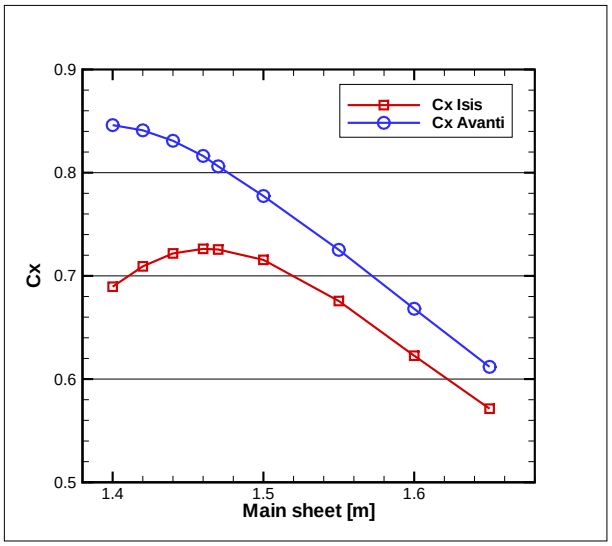

Figure 3. Cx **versus the main sheet length**

It is interesting to note that a maximum of Cx is found by ARA-ISIS at 1.46 m which is not the case for Cx values found by ARAVANTI. These differences come from the limitations of the inviscid flow solver. The inviscid flow code AVANTI does not take into account the viscous boundary layer, therefore, the prediction of the flow separation is not possible. Because of the twisted wind profile, the angles of attack at the head of sails are higher. Separated flow regions may exist on the sails' suction side near the head and trailing edge. When sails are trimmed in harder, the area of separated flow increases because of higher angle of attack, particularly at the top of the sails. The inviscid flow model in ARAVANTI ignores flow separation as an attached flow is imposed all the way to the trailing edge. According to sailors experience, the main sail flying shape for sheet length shorter than 1.45 m looks over-trimmed and the good main sheet trim in these conditions would be around 1.47 m.

It should also be noted that values of Cmx predicted by ARAVANTI and ARA-ISIS are very close (in the region of constant difference), while Cy is higher according to the viscous model ARA-ISIS. This is due to the differences in the vertical location of the centre of effort found by both coupled codes.

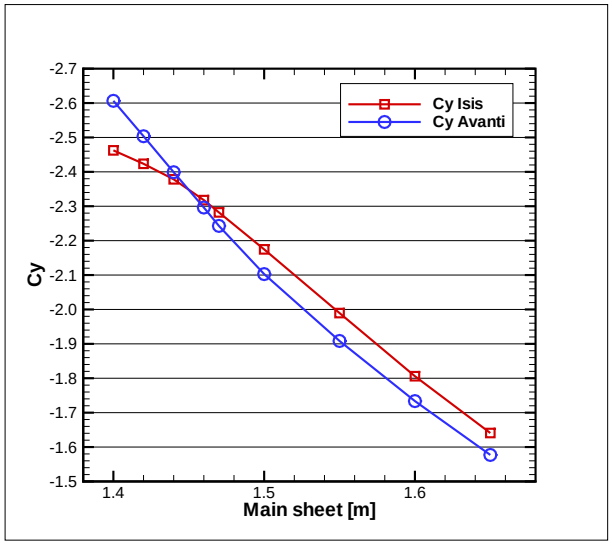

Figure 4. Cy **versus the main sheet length**

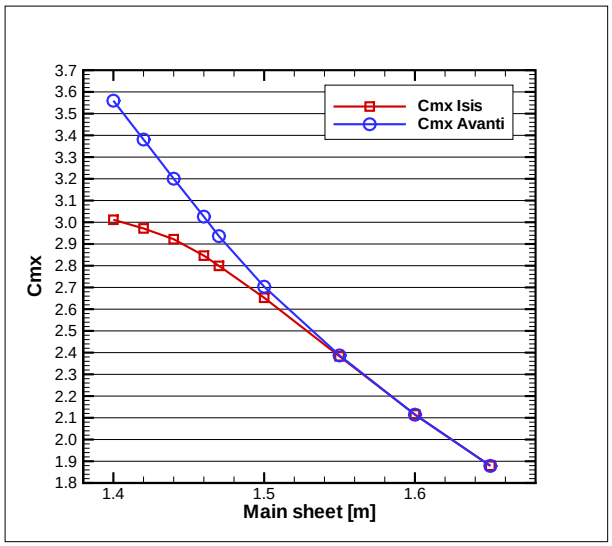

Figure 5. Cmx **versus the main sheet length**

Figure 6 presents the evolution of the centre of aerodynamic forces height ZCE for both coupled FSI tools, versus the main sheet length. It is the intersection between the central axis of the forces matrix and the (Z,X) absolute reference plan.

ZCE is higher according to ARAVANTI and it shows a monotonic increase when the sheet is hauled in, while ZCE has a maximum value at 1.5 m of the main sheet length, according to ARA-ISIS. The difference of location is about 0.4 m higher when the sheet is ease out, and about 1 m higher

when it is hauled in, according to ARAVANTI.

As explained previously, angles of attack increase when the sail is over trimmed in, particularly near the head of sails, which leads to an increase in the separation flow area (not modelled by the inviscid flow solver).

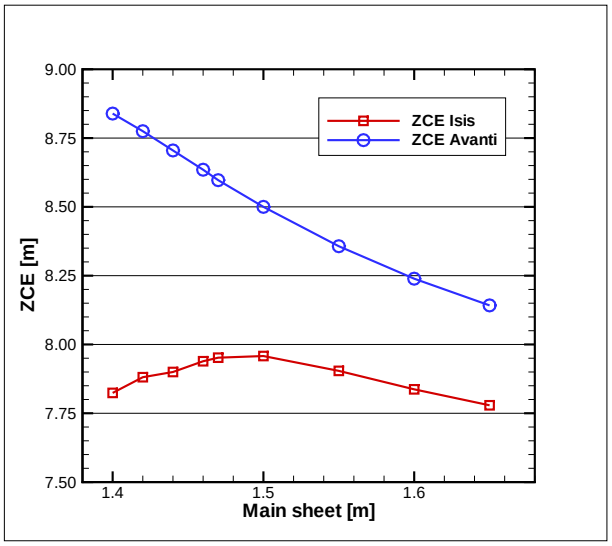

Figure 6. ZCE **versus the main sheet length**

3.2 $\triangle C_P$ and flying shapes

Two cases of main sheet trim are chosen in order to compare the differences on the sail shape and the difference of pressure between both coupled FSI solvers:

- $Trim_1 = 1.40$ m
- $Trim_2 = 1.60$ m

$\triangle C_P$ comparison

Figure 7 shows the projection of the flow velocity on the X axis for $Trim_1$ and $Trim_2$, on the sails' suction side. The flow on the main sail head suction side is separated when $Trim_1$ is used (see Figure 7 (a)). The Kutta condition is imposed at the leech of sails in the ARAVANTI simulations. Therefore, the separated flow is not computed, and differences between ARAVANTI and ARA-ISIS appear and increase while the main sheet is hauled in. With $Trim_2$, the flow on the suction side is attached (see Figure 7 (b)). $\triangle C_P$ results between the viscous and inviscid FSI solvers are expected to be close.

Figures 8 and 9 show $\triangle C_P$ versus the curvilinear abscissa computed by ARAVANTI and ARA-ISIS on the jib and the main sail, for both main sail trims $Trim_1$ and $Trim_2$ and for different heights.

Figure 8 shows the pressure difference on the jib. Both models predict very similar $\triangle C_P$ distributions. The peak computed at the leading edge by ARAVANTI is visible, but it is lower than the one found on the main sail. Suction values seem to be a little bit higher according to ARA-ISIS.

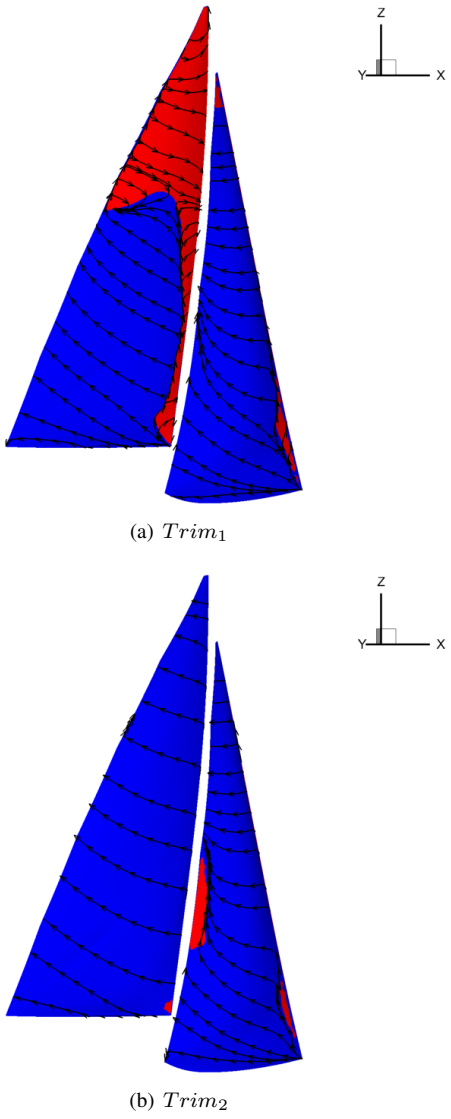

(a) $Trim_1$

(b) $Trim_2$

Figure 7. Sign of Vx computed with ARA-ISIS
Blue surfaces show the direct flow and red surfaces show the reverse flow.

Figure 9 shows the pressure difference on the main sail. For both $Trim_1$ and $Trim_2$, the highest difference is visible on the peak of $\triangle C_P$ at the leading edge of the main sail. Particularly with the ARAVANTI results for $Trim_1$, where the difference between both coupled FSI tools is increasing with height. With $Trim_2$, results seem to be very close between the inviscid and viscous flow solvers, except for the sharp suction peak of $\triangle C_P$ at the leading edge of the main sail.

Figures 10 and 11 show the evolution of $\triangle C_P$ integrated on the sails curvilinear abscissa versus height (see Equation (7)). Data are plotted for both $Trim_1$ and $Trim_2$ on the main sail (Figure 10) and the jib (Figure 11).

$$\Sigma_{\triangle C_P(z)} = \int \triangle C_P(z) \frac{\mathrm{dl}(z)}{\mathrm{l}_0} \tag{7}$$

With, $\mathrm{l}_0 = \sqrt{S_{ref}}$.

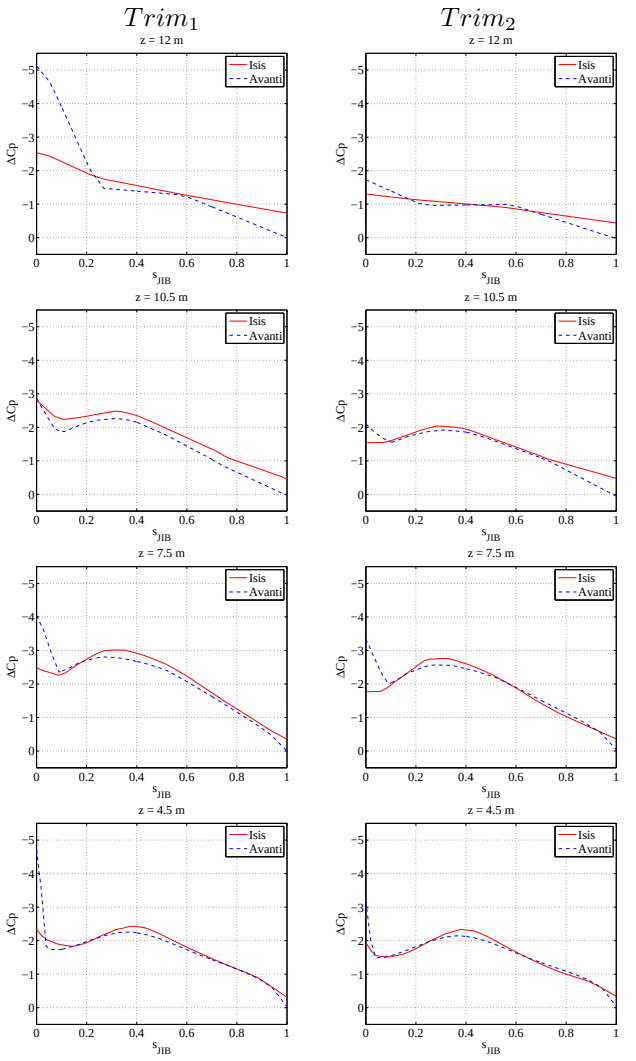

Figure 8. Jib $\triangle C_P$ along the height
Plots on the left correspond to the $\triangle C_P$ of $Trim_1$ for different heights, and plots on the right correspond to the $\triangle C_P$ of $Trim_2$ for several heights. The heights are 4.5 m, 7.5 m, 10.5 m and 12 m corresponding to the plots from the bottom to the top. The blue dashed lines represent the values found by ARAVANTI and the red continuous lines are the values found by ARA-ISIS. Curvilinear abscissa $s = 0$ and $s = 1$ for the leading and trailing edges respectively.

Figure 9. Main $\triangle C_P$ along the height
Plots on the left correspond to the $\triangle C_P$ of $Trim_1$ for different heights, and plots on the right correspond to the $\triangle C_P$ of $Trim_2$ for several heights. The heights are 4.5 m, 7.5 m, 10.5 m and 12 m corresponding to the plots from the bottom to the top. The blue dashed lines represent the values found by ARAVANTI and the red continuous lines are the values found by ARA-ISIS. Curvilinear abscissa $s = 0$ and $s = 1$ for the leading and trailing edges respectively.

Differences are clearly visible on the main sail with $Trim_1$, in particular for z values higher than 7.5 m in the separated flow area. With $Trim_2$, profiles are more similar, inviscid $\Sigma_{\triangle C_P}$ being a little bit higher, which is in accordance with previous results. The bottom point is the only one which is underestimated by ARAVANTI compared to ARA-ISIS.

For the jib, $\Sigma_{\triangle C_P}$ distributions are very similar and the tightest main sail trim leads to increases in the $\Sigma_{\triangle C_P}$ on the jib. Differences between both FSI coupled codes are clearly shown for the two bottom points, with both trims, where $\triangle C_P$ is under estimated by the inviscid flow solver.

In both inviscid and viscous models, a symmetry condition is imposed at the sea level, $z = 0$ m. The flow vortex at the sails foot level is not modelled in these inviscid FSI computations. Therefore, $\triangle C_P$ is underestimated at the foot levels and it leads to an increased ZCE. It would be interesting to allow vorticity emission at the sails foot (it is actually only allowed at the leech) and by varying the sea level in the viscous calculations, the boundary condition effects could be analysed.

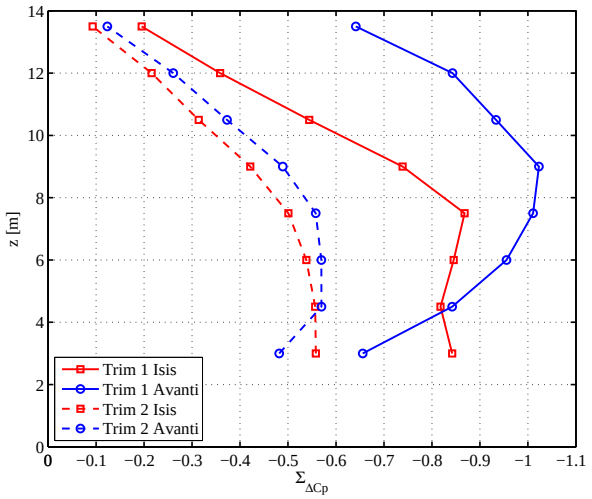

Figure 10. Main $\Sigma_{\triangle C_P}$

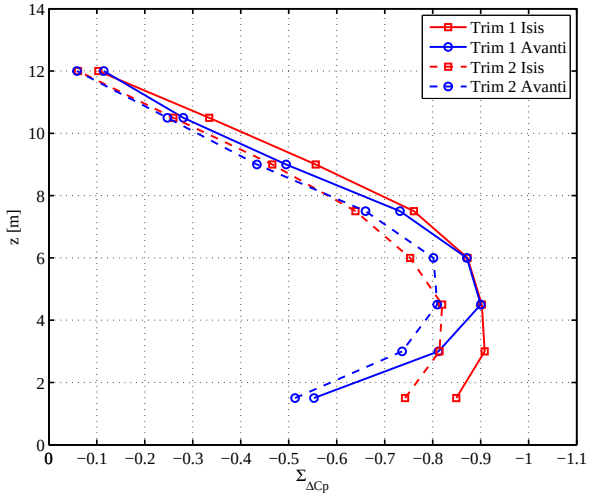

Figure 11. Jib $\Sigma_{\triangle C_P}$

ARA-ISIS versus height for $Trim_1$ and $Trim_2$. Except on the head of the sails, $Angle$ values are very close for the main sail and the jib when the trim used is $Trim_2$. The jib is a little bit more twisted for both cases of trim according to the ARAVANTI computations. For the case of $Trim_1$, ARAVANTI found higher values than ARA-ISIS for the main sail $Angle$. The difference is particularly high at the head: about 5-6 deg. The influence of the main sail trim on the jib head $Angle$ is also visible. It decreases when the main sheet is eased out (about 3-4 deg).

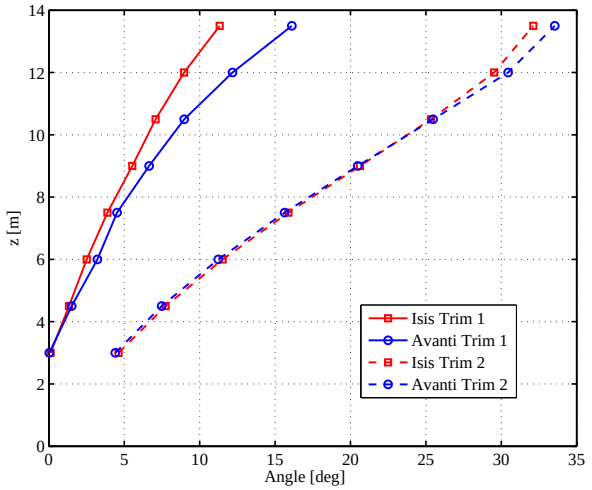

Figure 12. Main *Angle*

Flying shapes comparison

The differences on the shapes computed by both FSI tools are studied by using two parameters: $Angle$ and $Camber$.

$Angle$ is the angle in degrees between the chord of the studied sail and the longitudinal axis of the boat.

$Camber$ is the camber value of the studied sail in percentage of the chord length.

Figures 12 – 15 present the $Angle$ and $Camber$ results while Figure 16 shows the flying shapes of sails and structures for both trims and inviscid/viscous calculations.

Figures 12 and 13 show the evolution of the $Angle$ of the main sail and the jib, computed by ARAVANTI and

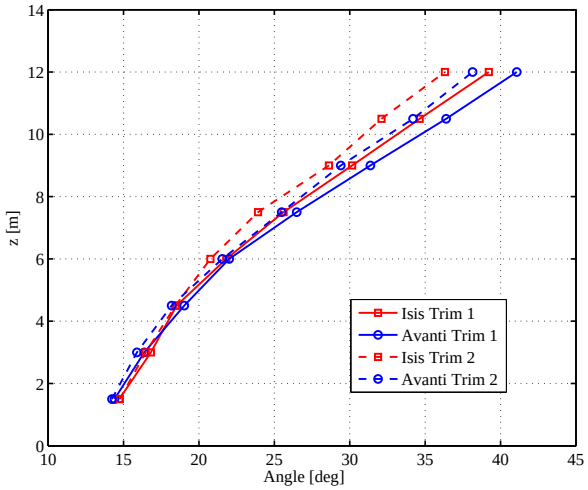

Figure 13. Jib *Angle*

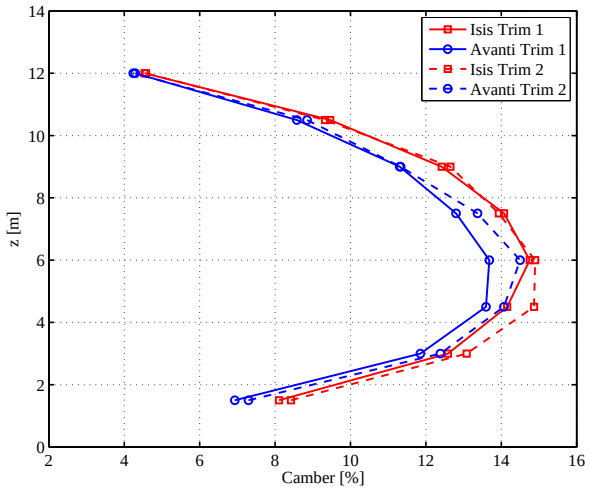

Figure 15. Jib *Camber*

Figures 14 and 15 show the evolution of the main sail and jib $Camber$, computed by ARAVANTI and ARA-ISIS versus height for $Trim_1$ and $Trim_2$. ARAVANTI found a lower $Camber$ than ARA-ISIS on the jib for both cases of main sheet length (see Figure 15). This is particularly visible on the middle height of the jib.

When the main sheet length is $Trim_2$, ARAVANTI found a higher value of $Camber$ for the main sail and the difference is close to constant starting from $z = 6$ m until $z = 12$ m (see Figure 14). When the main sheet length is $Trim_1$, ARAVANTI and ARA-ISIS compute a very close main sail $Camber$ until $z = 7.5$ m. Starting from 7.5 m, the difference between the two calculations increases and ARAVANTI gives a main sail with a higher camber (see Figure 14). This difference appears in the recirculation area of the main sail.

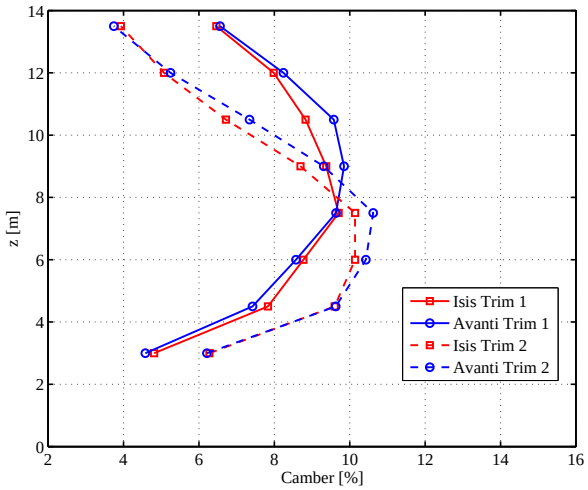

Figure 14. Main *Camber*

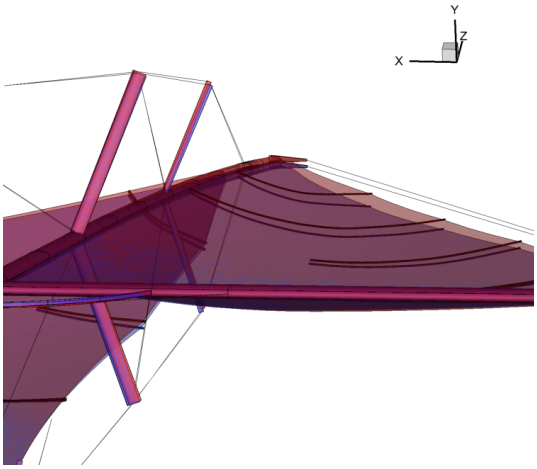

(a) $Trim_1$

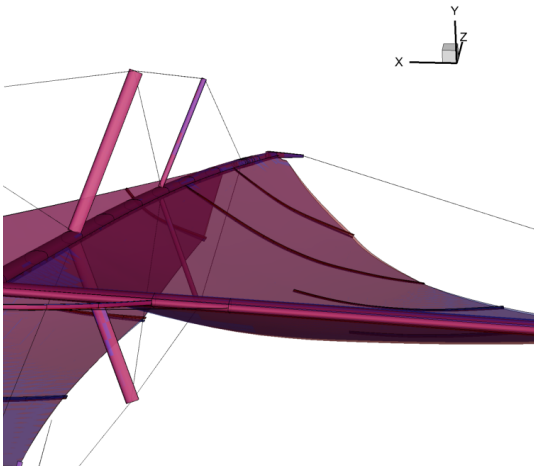

(b) $Trim_2$

Figure 16. Shapes visualisation
Blue and red shades show the ARAVANTI inviscid) and ARA-ISIS (viscous) calculations

4. TRIMMING OPTIMISATION

4.1 Optimisation method

An optimisation procedure has been tested in order to optimise the sail trimming in the case of low true wind speed. In this specific case, the maximum righting moment is not a constraint as the heel angle is easily controlled. Hence, a rapid optimisation of sails trim can be based on a simple objective function defined only with the aerodynamic driving and side forces. This simple procedure is expected to be much less expensive than the use of a full VPP which needs hydrodynamic forces to be determined. The objective function to maximise is the driving force with a penalty due to the side force which induces an added hydrodynamic drag and leeway. In this work, we define this function F_{obj} as:

$$F_{obj} = F_x + 0.05F_y \tag{8}$$

Where the aerodynamic side force Fy is negative. Different values of the side force penalty coefficient have been tested and a value of 0.05 appeared to be a reasonable compromise. An accurate estimation of this coefficient would require a thorough hydrodynamic investigation, but a rapid preliminary one showed that the chosen value was consistent for the Figaro class yacht.

The boat speed is fixed to 4.8 kts, the true wind speed at 10 m height is 8 kts and the true wind angle is equal to 40 deg port-side. The trim, heel and heading angles are 0, 10 and 0 deg respectively. Two parameters of trimming are optimised: the main sheet length (number 1 on Figure 17) and the main car length (number 2 on Figure 17).

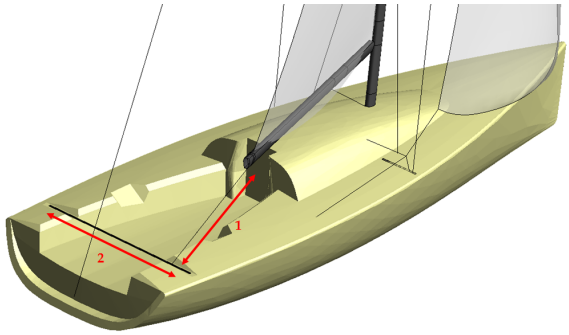

Figure 17. Main sail trimming

An optimisation method has been programmed in order to maximise F_{obj}. The optimisation algorithm is based on the "Generalized Pattern Search Method (GPS)" which is a generalisation of the Hooke and Jeeves method [23]. This method consists in a series of displacements around a central evaluation point (also called "Pattern"). At each iteration, the objective function is evaluated on the points of the Pattern. If an improvement is found, the associated point becomes the new central evaluation point. The size and the orientation of the Pattern can be adapted at each Pattern iteration, in order to accelerate convergence. The methods used are the "Opportunistic and Dynamic Run" [24], which leads to a decrease in the computing time.

The optimum point is calculated with the inviscid FSI solver and some points near the "inviscid optimum" are also evaluated with the viscous FSI solver, by using the same numerical set-up, according to this case of low true wind speed, in order to compare the "inviscid" and "viscous optima".

4.2 Optimisation results

An optimisation algorithm has been coupled to the inviscid FSI solver ARAVANTI in order to maximise the objective function F_{obj} (defined with Equation (8)) by optimising the trimming of the main sail. The GPS algorithm has been used and results are plotted on Figures 18 – 20. The "inviscid optimum" trimming is found after 20 iterations.

Figure 18 shows the interpolated contours of the 20 evaluations versus both main sheet and car lengths. The response surface is created with "Augmented Radial Basis Functions" methods [25] and the "Thin Plate" function is used (see Equations (9 – 10)).

$$F_{obj_{interp}}(x) = \sum_{j=1}^{n} \lambda_j \phi(\parallel x - x_j \parallel) + \sum_{k=1}^{m} \gamma_k p_k(x) \tag{9}$$

$$\phi(r) = r^2 \log r \qquad (r \geq 0) \tag{10}$$

The weights λ_j and γ_k are solved with the conditions:

$$F_{obj_{interp}}(x_j) = F_{obj_j}$$

$$\sum_{j=1}^{n} \lambda_j p_k(x_j) = 0$$

A dashed black line has been added which represents the middle position of the main car. Figure 19 shows the inviscid and viscous RBF interpolated F_{obj} versus the main sheet length with a main car fixed at 0.2 m to leeward.

The "inviscid optimum" trim is found for a main sheet of 1.45 m and a main car of 0.2 m. The main sheet has more influence on F_{obj} than the main car. Four points (black squares) have been calculated with the viscous FSI solver near the "inviscid optimum", by varying the main sheet only. These points show that the viscous F_{obj} at the "inviscid optimum" are lower than the inviscid F_{obj}. It is about 555 N for the "inviscid optimum" and 409 N for the same trim computed with the viscous solver. These differences come from the limitations of the inviscid flow solver that has been shown previously. It should also be noted that the optimum point found by ARA-ISIS (viscous) is more eased out for the main sheet than the one found by ARAVANTI (see Figures 18 and 19). The "viscous optimum" leads to a value of 1.48 m according to ARA-ISIS while it is 1.45 m according to ARAVANTI.

Figure 20 shows the sign of Vx on the sails' leeward surface calculated by ARA-ISIS for the "inviscid optimum" trim. The red color shows the separated area which is not modelled by the inviscid calculations. This leads to differences between both models.

These results show the difficulties faced by an inviscid FSI solver when an optimisation trimming procedure is used in a case of low true wind speed. This specific case is the worst case for the inviscid FSI trimming optimisation as the real flow is significantly separated at the real optimal trim. In heavier winds, the optimal trim is less tight because the penalty of the heeling moment becomes dominant. Hence, flow separation at the optimal trim is reduced, making the inviscid flow model more appropriate. An optimisation in stronger winds should consider the heeling moment in the objective function.

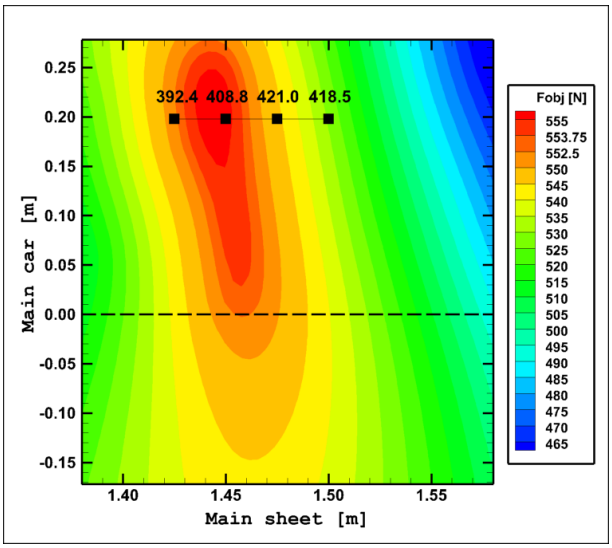

Figure 18. Optimum trim
Negatives values: windward side
Positives values: leeward side

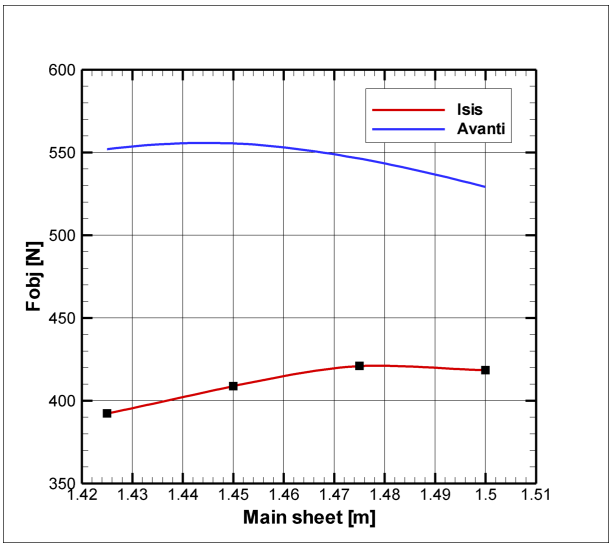

Figure 19. Optimum trim (main car fixed at 0.2m)

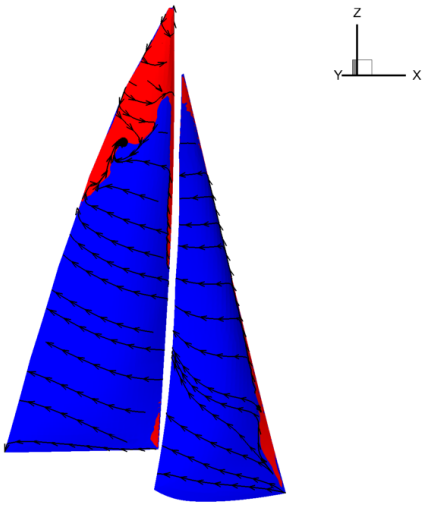

Figure 20. Sign of Vx for the "inviscid optimum" trim computed with ARA-ISIS
Blue surfaces show the direct flow and red surfaces show the reverse flow.

5. CONCLUSIONS

A comparison between FSI models with either an inviscid or a viscous fluid solver applied to a Figaro Class yacht has been achieved. Differences on the aerodynamic coefficients and the sails' flying shape have been studied for different values of the main sheet length.

The ARAVANTI model (finite element model ARA, coupled to the inviscid flow model AVANTI), has shown very close results compared to the ARA-ISIS model (finite element model ARA, coupled to the URANS ISIS-CFD model), when the main sheet has not been over trimmed. In this case, the driving force was 7% higher and the heeling force 4% lower according to the ARAVANTI results. The heeling moment found was very close between both models. In the case of over trimmed main sheet, all coefficients have been overestimated by ARAVANTI.

The evolution of $\triangle C_P$ between both FSI tools versus height has been shown. The differences in the shapes of the sails has shown an interesting link with the separation region for the main sail. Differences in the twist of the main sail were large for the over-trimmed case: about 5 degrees difference on the head compared to an $Angle$ value of 11-12 degrees. ARA-ISIS found higher cambers for the jib in both cases of trim. For the main sail, cambers were higher according to ARAVANTI. The difference on the $Camber$ has been particularly visible for the over-trimmed case, where ARA-ISIS predicts a reduction of $Camber$ on the separated flow region, which has not been the case of the ARAVANTI result.

The difficulty of using an inviscid flow solver in order to optimise the sail trimming has been shown. An investigation, for a case of low true wind speed, has been performed by using an inviscid FSI optimisation procedure to optimise the main sail sheet and car trim in order to maximise an objective

function based on the driving and side forces. Unfortunately, the optimum point has been found to be a little bit too trimmed in; the same case computed by ARA-ISIS has shown significant flow separation and differences in the optimum point location. It should be noted that ARAVANTI leads to an "inviscid optimum" trim which is near the "viscous optimum", and it can be used as a first level model in a multi-model optimisation for saving time. The code is also able to show the influence of each type of trimming on forces and flying shapes.

For the future work, the uncertainty in the different meshes (fluid and structure) should be computed. This will lead to improvements in the results reliability, and the evolutions of the inviscid and viscous differences will be evaluated. It should also be interesting to work on suction peak models which can be implemented in ARAVANTI in order to increase the accuracy. Investigations on the optimisation of the trimmings are in development. A new optimisation method based on the heeling moment is currently being tested. The method leads to interesting results with ARAVANTI. A hydrodynamic matrix of the Figaro Class yacht has been calculated. Data will be used for a future VPP in order to investigate the optimisation of the trim.

Acknowledgements

The authors wish to acknowledge the *All Purpose*, *BSG Développements*, and *Sparcraft* companies, for shared informations. The authors are also grateful to the Figaro sailor Gwénolé Gahinet for discussions.

References

[1] M. Durand. *Interaction fluide-structure souple et légère, application aux voiliers*. PhD Thesis, Ecole Centrale de Nantes, 2012.

[2] W. Menotti, M. Durand, D. Gross, Y. Roux, D. Glehen, and L. Dorez. An unsteady FSI investigation into the cause of the dismating of the Volvo 70 Groupama 4. In *INNOVSail, Innovation in high performance sailing Yacht*, page 197, Lorient, 2013.

[3] D. Trimarchi. *Analysis of downwind sail structures using non-linear shell finite elements*. PhD Thesis, University of Southampton, 2012.

[4] B. Augier. *Etudes expérimentales de l'interaction fluide-structure sur surface souple: application aux voiles de bateaux.* PhD Thesis, Universite de Bretagne Occidentale, 2012.

[5] B. Augier, P. Bot, F. Hauville, and M. Durand. Experimental validation of unsteady models for fluid structure interaction: Application to yacht sails and rigs. *Journal of Wind Engineering and Industrial Aerodynamics*, 101: 53–66, 2012.

[6] P. V. Oossanen. Predicting the Speed of Sailing Yachts. *SNAME*, 101:337–397, June 1993.

[7] R. Korpus. Performance Prediction without Empiricism: A RANS-Based VPP and Design Optimization Capability. In *The 18th Chesapeake Sailing Yacht Symposium, SNAME*, 2007.

[8] H. Hansen, P. S. Jackson, and K. Hochkirch. Real-time velocity prediction program for wind tunnel testing of sailing yachts. *Proc. The Modern Yacht, Southampton, UK*, 2003.

[9] Y. Masuyama and T. Fukasawa. Full scale measurement of sail force and the validation of numerical calculation method. In *The 13th Chesapeake Sailing Yacht Symposium, SNAME*, 1997.

[10] Y. Masuyama, Y. Tahara, T. Fukasawa, and N. Maeda. Dynamic performance of sailing cruiser by a full scale sea reality. In *The 11th Chesapeake Sailing Yacht Symposium, SNAME*, 1993.

[11] K. Roncin. *Simulation dynamique de la navigation de deux voiliers en interaction*. PhD Thesis, Ecole Centrale de Nantes, 2002.

[12] L. Huetz. *Systematic study of the hydrodynamic behaviour of sailing yacht hulls using CFD and parametric design*. PhD Thesis, Ecole Centrale de Nantes, 2012.

[13] L. Huetz and P. E. Guillerm. Database building and statistical methods to predict sailing yacht hydrodynamics. *Ocean Engineering*, 90:21–33, 2014.

[14] N. Rousselon. Optimization for sail design. In *modeFRONTIER Conference*, 2008.

[15] M. A. Abramson, C. Audet, and J. Dennis. Design optimization of interacting sails through viscous CFD. In *INNOVSail, Innovation in high performance sailing Yacht*, Lorient, 2003.

[16] R. Ranzenbach, D. Armitage, and A. Carrau. Mainsail Planform Optimization for IRC 52 Using Fluid Structure Interaction. In *The 21st Chesapeake Sailing Yacht Symposium, SNAME*, 2013.

[17] Y. Roux, M. Durand, A. Leroyer, P. Queutey, M. Visonneau, J. Raymond, J. M. Finot, F. Hauville, and A. Purwanto. Strongly coupled VPP and CFD RANSE code for sailing yacht performance prediction. In *3rd High Performance Yacht Design Conference Auckland, 2-4 December*, pages 215–225, Auckland, 2008.

[18] Y. Roux, S. Huberson, F. Hauville, J. P. Boin, M. Guilbaud, and B. Malick. Yacht performance prediction : Towards a numerical VPP. In *1st High Performance Yacht Design Conference Auckland, 4-6 December*, Auckland, 2002.

[19] I. M. Viola, P. Bot, and M. Riotte. On the Uncertainty of CFD in Sail Aerodynamics. *International Journal for Numerical Methods in Fluids*, 72(11):1146–1164, 2013.

[20] F. R. Menter, M. Kuntz, and R. Langtry. Ten years of industrial experience with the SST turbulence model. *Turbulence, heat and mass transfer*, 4:625–632, 2003.

[21] R. G.J. Flay. A twisted flow wind tunnel for testing yacht sails. *Journal of Wind Engineering and Industrial Aerodynamics*, 63(1):171–182, 1996.

[22] F. Fossati. *Aero-Hydrodynamics and The Performance of Sailing Yachts*. International Marine / McGraw-Hill, 2009.

[23] R. Hooke and T. A. Jeeves. Direct search solution of numerical and statistical problems. *Asso C. Computing Machinery J.*, 8:212–229, 1960.

[24] M. A. Abramson, C. Audet, and J. Dennis. Generalized Pattern Search Algorithms : unconstrained and constrained cases. In *IMA Workshop*, 2003.

[25] G. B. Wright. *Radial Basis Function Interpolation: Numerical and Analytical Developments*. PhD Thesis, University of Colorado, 2003.